ANALYSIS AND VALIDATION OF HETEROGENEOUS DYNAMIC RUPTURES MODELED BY EARTHQUAKE CYCLE SIMULATION

A. Petukhin [(1)], P. Galvez [(2,3)], P. Somerville [(4)], K. Miyakoshi [(5)], K. Irikura [(6)]

(1) Senior researcher, Geo-Research Institute, earthquake engineering, Osaka, Japan, anatolyp@geor.or.jp
(2) Visiting researcher, ETH Zurich, Earth Science, Switzerland, percy.galvez.barron@gmail.com
(3) Researcher, KAUST University, Saudi Arabia, percy.galvez.barron@gmail.com
(4) Principal Seismologist, AECOM, Los Angeles, United States, paul.somerville@aecom.com
(5) Group leader, Geo-Research Institute, earthquake research, Osaka, Japan, ken@geor.or.jp
(6) Adjunct Professor, Aichi Institute of Technology, Japan, irikura@geor.or.jp

Abstract

Physics-based dynamic rupture modelling is necessary for estimating parameters such as rupture velocity and slip rate function that are poorly resolved by seismic source inversion. In order to generate a large number of physically self-consistent rupture models, whose rupture process is consistent with the spatio-temporal heterogeneity of past earthquakes, we use multicycle simulations under the rate-and-state (RS) friction law. We performed a parametrization study by fully dynamic rupture modeling, and then, a set of spontaneous source models was generated in a wide magnitude range (*Mw*5.5-8.0) [1].

In order to validate rupture models, we compare the source scaling relations vs. seismic moment *Mo* for the modeled rupture area *S*, as well as average slip *Dave* and the slip asperity area *Sa*, with similar scaling relations from the source inversions. Ground motions were also computed from our models. Their peak ground velocities (*PGV*) agree well with the GMPE values. We obtained good agreement of the permanent surface offset values with empirical relations.

From the heterogeneous rupture models, we analyzed distributions of slip, slip rate, rupture initiation points, rupture velocities, and source time functions. We studied cross-correlations between them and with the friction weakening distance *Dc* value, the only initial heterogeneity parameter in our modeling. The main findings are: (1) high slip-rate areas are coinciding with or located on an outer edge of the large slip areas, (2) ruptures have a tendency to initiate in small *Dc* areas, and (3) high slip-rate areas correlate with areas of small *Dc*, large rupture velocity and small rise-time.

Keywords: earthquake dynamics, source characterization, strong ground motion prediction

1. Introduction

Physics-based dynamic rupture models can be used for verification of assumptions underlying strong ground motion simulation schemes (e.g. Recipe [2]) and for constraining seismic source inversion. To enable the generation of physically self-consistent initial parameters for dynamic rupture models that are consistent with the heterogeneous distribution of fault strength and fault geometry, in the companion study [1] we employ earthquake cycle modeling. Our approach involves producing earthquakes based on the rate-and-state (RS) friction law in order to examine the impact of assumed friction model.

A single RS simulation that spans about several thousand years can generate multiple scenario earthquakes with spatio-temporal complexity similar to past earthquakes. A limited number of RS cycle models can thereby provide a sufficiently large database of moderate-to-large earthquakes. Most importantly, individual events are not the results of ad hoc tuning of stress and strength heterogeneities; they are the results of the spatio-temporal evolution of the governing parameters on the frictional interface in response to steady plate loading. This helps us getting well validated event dataset that can be used to investigate the dynamic rupture characteristics of each single event, which may be poorly resolved by source inversion, e.g.: spatial correlation of high slip and high slip-rate areas, source time functions, rupture velocities, etc. [3, 4].

Target for this study is the magnitude range of transition between 1st and 2nd stages ("self-similar" and "width-saturated" ruptures, *Mw* = 5.5-6.5 and 6.5-7.5) of the 3-stage scaling proposed in [2]. The seismogenic zone width *Wseis* plays a fundamental role in the 1st to 2nd stage transition. In [5] this transition is assigned to effect of *Wseis* based on numerical model [6]. Tectonic loading with viscous-elastic asthenosphere is important feature of this modelling that allow transition under constant stress drop. Contrary, in [7] reported that events which break the whole seismogenic width and reach the free surface are exposed to an attraction effect from the free surface. This attraction effect may explain the transition regime from stage 1 to stage 2 too.

The heterogeneity of each rupture parameter can be described by an auto-coherence function (ACF) while the linear dependency between parameters is described by a cross-coherence. For example, in [8] it is found that heterogeneity of earthquake slip of past events is described by von Karman ACF. [9, 10] extend the analysis to the cross-coherence that controls the linear dependency between parameters including non-zero offset coherence as well as zero offset. They found that coherence with non-zero offset may exist between slip and other temporal rupture parameters, such as peak slip rate, rupture velocity and rise time. This kind of result can be used to characterize rupture kinematics of earthquakes for the improvement of kinematic ground motion simulation methods.

Main targets of this study are: (1) validating rupture models from [1], and (2) based on this well validated set of simulated ruptures explore kinematic parameters that are poorly estimated by seismic source inversion, i.e. rupture velocity (*Vr*) and stress drop ($\Delta\sigma$), as well as their spatial cross-correlations with peak slip rate (*PSR*, primary parameter for strong motion prediction) and with *Dc* (the only heterogeneous friction parameter underlying earthquake cycle modelling). For validation we will use source scaling relations, permanent surface offset and ground motions, which are well constrained by observations. Also, we will explore slip rate functions (SRF), parametrize them by fitting regularized Yoffe function (RYF, [11]) and compare spatial distribution of RYF parameters with spatial distributions of other key parameters: *PSR* and *Dc*.

2. Screening of simulated ruptures

In our best model [1] we generated about 100 events. In order to be consistent with observed (inverted) source models, which usually have subfault size 1-2km, and to get enough resolution at the same time, we converted original rupture models, having 125 m mesh, to the 1km mesh for ruptures *Mo* > 2e18 Nm or to the 0.5 km mesh for ruptures *Mo* < 2e18 Nm. The simulated events span a magnitude range of *Mw* = 5.5-7.5 (e.g. see Fig.1) that correspond to transition between 1st and 2nd stages in the source scaling relationship

assumed in [2]. Examples of distribution of the peak slip, *PSR*, rupture time and Δσ are shown in Fig.9 below.

Unfortunately, some ruptures have unnatural artefacts. E.g., double ruptures that can be distinguished by analysis of the rupture time distributions [1, Fig.6a]. Other doubtful ruptures are those covering whole area of the fault model, but not arrested by the large *Dc* barriers. We made careful screening of rupture models and deleted such ruptures from our analysis; 10% in total.

We found that ruptures of some events have large peak slip velocities appearing at the edge of the fault plane, see example in [1, Fig.6b]. However, for natural earthquakes this type of rupture is very rare extreme case; in past earthquakes there were no cases that SMGA, which is interpreted as the area of high slip rate, is located on the edge of fault. We name such events as the "edge-arrested ruptures" and other events as the "self-arrested ruptures" respectively. For reliability, we also remove edge-arrested ruptures (5%) from this analysis. We should notice that edge-arrested ruptures belong to the largest-Mw segment of the set of ruptures, while our primary target is the transition between 1st and 2nd stages in *Mw*6-7 range.

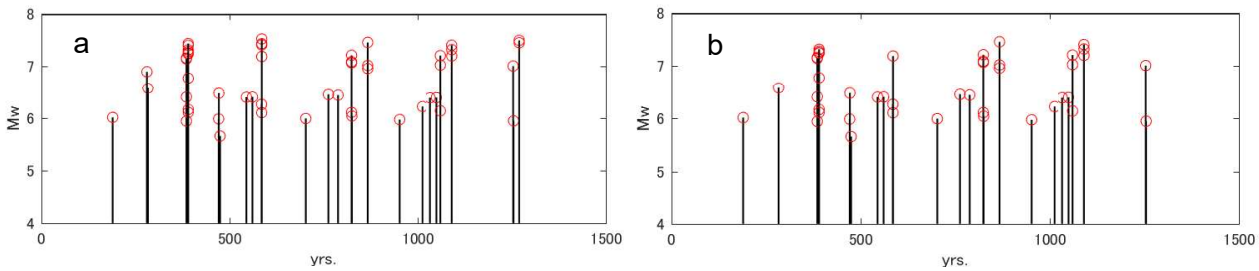

Fig. 1 – Time series of simulated events. First 200 years is the loading and warm-up stage where no events were generated. Both cases before (a) and after (b) the screening for repeating earthquakes are shown for comparison

Another simulation artefact rises from the fact that the threshold 0.1 m/s to switch from quasi-dynamic simulation to the fully dynamic simulation in [1] may be crossed several times during the same quasi-dynamic rupture initiation. As result, we have clusters of several fully dynamic ruptures with a slightly different initial conditions in the rupture initiation zone. In most cases these ruptures have pattern very similar to the first event in cluster; we manually check and remove such events from analysis (another 35%) and keep only the first event, compare Fig.1a and b. However, in some cases, rupture pattern may significantly differ from the previous event in a cluster. In order to increase statistics of models, while keeping low computation cost, we preserve such ruptures in analysis.

3. Validation of rupture models

In order to have reliable set of ruptures that will allow us to make reliable conclusions, we validate rupture models by comparison of simulated and observed source scaling, ground motions (GMPE), and permanent surface offset. On the simulation stage we tuned friction parameters in such a way to get well validated models: tune stress drop to get proper scaling relationship, tune max *Dc* to get proper *Vr* and ground motions respectively, tune near surface settings to get reasonable permanent surface offset. As well we tune correlation length of *Dc* heterogeneities in order to get realistic irregular seismic regime (irregular for Stage 1 and 2 but may be characteristic for Stage 3). In order to analyze irregularity of seismic regime we plot ruptures vs. time and *Mw*; see Fig.1b.

3.1 Source scaling relationships

Criteria and trimming procedures, proposed in [12], are used to estimate rupture area *S*, asperity area *Sa* and average slip *Dave*. Scaling of *S* and *Dave* vs. seismic moment *Mo* is shown in Fig.2. Gradient of *S*-values clearly show existence of transition between Stage 1 and Stage 2. This is in accordance with assumption [13],

that transition of scaling is due to transition from self-similar ruptures to ruptures having saturated width (W-model). Assumption of [7], that due to mirror effect surface rupturing largely increases *Dave* and *Mo* respectively, while *S*-increase is minor, probably results mainly in step-like change of scaling relationship at transition point. Notice that transition of scaling was observed also in Cases 1-4 in [1] that have no surface ruptures. By tuning normal stress and *Dc* values in [1] we succeed to get good fit of absolute values of *S* too. Scaling of *Dave* vs. *Mo* also show existence of transition between Stage 1 and Stage 2, and absolute values of *Dave* also fit observations.

Earthquake ruptures are heterogeneous. Recipe [2, 13] is modeling rupture heterogeneity through the modeling of slip asperities. They employ results [12] for the scaling of area of slip asperities *Sa* vs *Mo*. In order to make validation of our simulated rupture models we also calculate scaling of *Sa* vs *Mo* and compare with observed scaling from [12]. Results are shown in Fig.3a. Total area of asperities *Sa* fit observed scaling very well, but number of asperities is underestimated. Most of ruptures have only one asperity, while average number of asperities in [12] is 2.6. Additional studies both on rupture modelling and seismic source inversion is necessary to understand this difference.

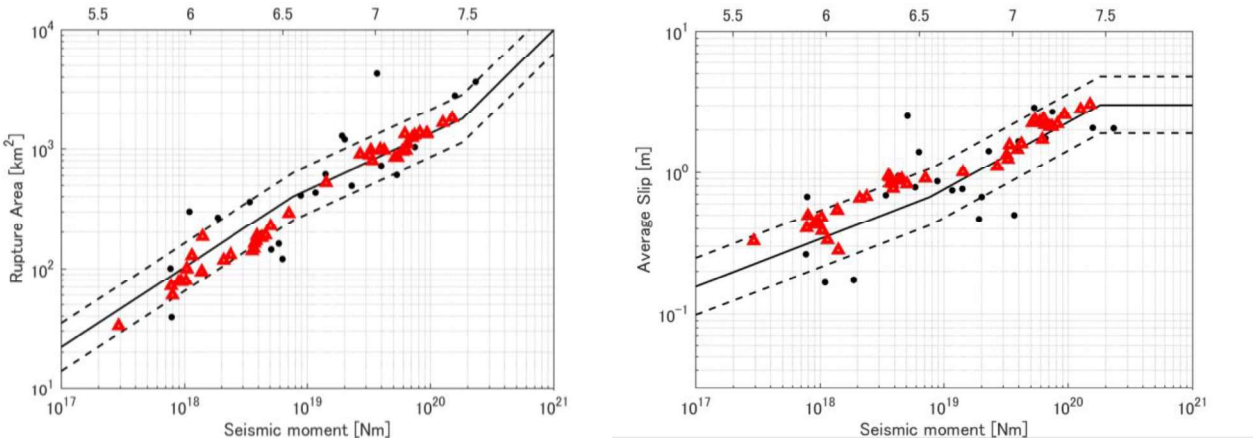

Fig. 2 – Scaling of the rupture area *S* (left) and average slip *Dave* (right). Red triangles are the simulated, and black dots are the observed ruptures. Line is 3-stage scaling [2]

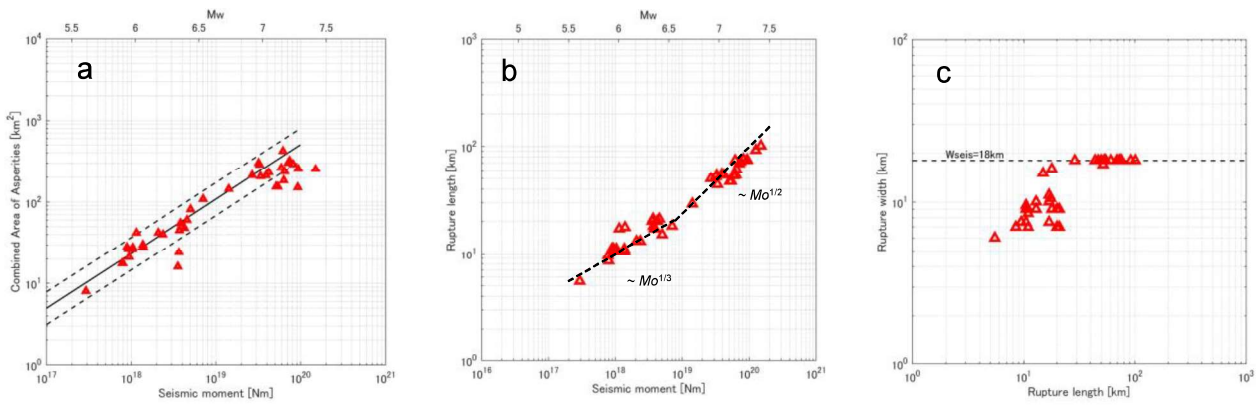

Fig. 3 – Scaling of the combined area of asperities *Sa* (a), rupture length *L* vs *Mo* (b) and rupture width *W* vs *L* (c). Line is scaling of [12], adopted by Recipe. *Wseis* = 18km is a typical seismogenic depth in Japan

Finally, Fig.3bc shows scaling for rupture length *L* and rupture width *W*. Due to setting of seismogenic width to *Wseis* = 18km, *W*-values vs *Mo* in the large magnitude 2nd stage, are saturated at *W* = 18km. Scaling of *L* vs *W* also has transition at *Mw* = 6.5 in accordance with Recipe assumption [13]. Trend vs. *Mo* well agree with supposed by Recipe too, Fig.3b.

3.2 Strong ground motions

In order to validate earthquake source models and strong ground motion prediction methodologies, validation "in average" by comparison with GMPEs is used widely (e.g. [14]). In this study we will validate earthquake cycle models by comparison of *PGV*'s of the simulated records and GMPE values.

3.2.1 Method of validation

We simulated ground motion waveforms for the modeled events without making any modifications to their source characteristics. We use the sources generated by the dynamic models and simulate waveforms using separate wave propagation software. Due to the large number of cells (up to 300000 for a *Mw*7.0 event) we used the staggered grid 3D-FDM method [15] (see also [16]) instead of the discrete wavenumber method [17], which is widely used for 1D velocity structures.

In order to reduce simulation time, which is necessary for the short-period simulations of many models in this study, we made simulations for velocity model that could be typical for hard rock sites. These sites are also typical for the critical engineering facilities, like the NPP's, improvement of the strong ground motion prediction recipe for which is the main target of this project. However, near surface velocity of *S*-wave shouldn't be out of the range allowed by the GMPE's, i.e. $Vs < 1500$m/s (e.g. [18]). Assumed velocity model for hard rock sites is an average 1D model for rock sites in the mountainous Chugoku region in Japan (34.5-35.5°N, 132.0-135.0°E), extracted from the JIVSM model [19]. Shallow layer of JIVSM model in this region, which is important for simulation of short-period waves, is tuned by the waveform simulation and well validated [20].

For all rupture models we simulated waveforms at the 4.4 km horizontal mesh, within 50 km from the fault. FDM grid size is 220 m; time step 0.0125 sec, duration of simulated waveforms is 75 sec, which should be enough to simulate *S*-wave segment within 50 km from source. The shortest period resolved by our FDM simulations is 1.0 sec. In order to extend frequency range to high frequencies, we applied hybrid method, combining deterministic and stochastic waveforms. Simulated *PGV* values are peak values in range 0.1-10 Hz. Observed data are GMPE for *PGV* values [21]. As a measure of distance, GMPE uses *Rrup* - the shortest distance to the rupture. We calculated *Rrup* as the distance from a target mesh to the nearest subfault of the rupture (source) model.

3.2.2 Validation results

Average synthetic/GMPE ratios for *PGV* values and their standard deviations are shown in Fig.4. There are no systematic discrepancies of average ratios of *PGV* that means that validation by comparison of simulated and observed ground motions is successful. Additionally, we tried to make comparison with recent GMPE of [18] (not shown here). Results are almost the same, but *PGV* values in [18], a little smaller than *PGV* in [21].

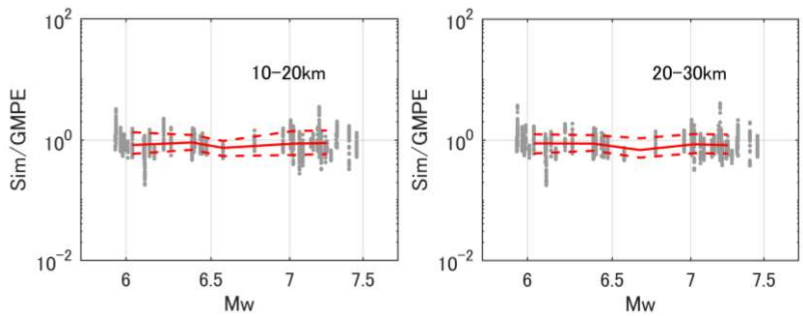

Fig. 4 – Average and *std*'s (red lines) of the *PGV* ratios (grey dots) in 2 distance ranges

3.3 Permanent surface offset

Easily measured after an earthquake by geological, GPS and recently by space interferometry methods, the permanent surface offset is one of the most reliably observed parameter of the earthquake rupture. Physics based models must reproduce it too. Moreover, by comparison of surface offsets for different friction models in companion study [1], we noticed that surface offset has better sensitivity to shallow friction settings ($H < 3$ km) than source scaling or ground motions. E.g., models with and without shallow cohesion have approximately the same $S(Mo)$ scaling and PGV ratios, while surface offset is almost zero in models with excessive cohesion and comparable with observed for models without cohesion.

Surface offset values for dynamic rupture models are calculated as the maximum slip in the row of the 1x1 km subfaults at zero depth. Some researchers (e.g. [22]) use slip value in the middle of surface rupture. We tested them too; however, for smooth ruptures in our dynamic models, these values are almost identical. For observed data we use re-examined data for the strike-slip events of [23] from [24].

Results of comparison are shown in Fig.5. Our simulation results (red triangles) are compared with observed data (black dots) and two scaling relationships for the West USA [22] and Japan. Simulation results correlate well with observed data, although slightly different from both scaling relationships. Simulated values at the 1st stage below $Mw6.5$ quickly decrease to zero with decreasing of Mw, in accordance with the self-similar model of ruptures that do not reach the surface. Most of ruptures that have non-zero surface offset belong to the 2nd stage of scaling relationship in accordance with W-model. Surprisingly, but surface offset values approximately equal to the $Dave$ values in the 2nd stage.

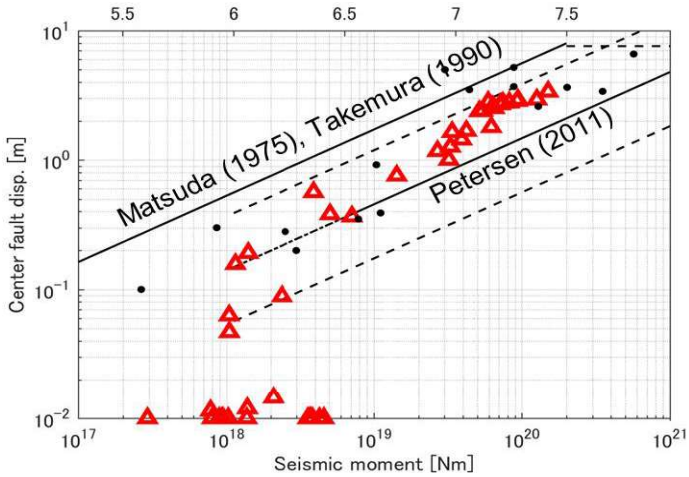

Fig. 5 – Comparison of simulated (triangle) and observed (dot) values of the permanent surface offset

4. Distribution of rupture initiation points

We start analysis of heterogeneous ruptures, validated above, from analysis of their initiation points. In the strong ground motion prediction through kinematic models, setting of rupture initiation is responsible for the directivity effect to the target site. The question that we address here if there is any preferable area(s) in cycles, where heterogeneous ruptures are initiating, or are they totally random?

Rupture initiation point is defined as a median center of area having minimal rupture time. In Fig.6a we compare location of rupture initiation points, with Dc distribution, the only heterogeneous friction parameter that reflect fault properties and prevail in cycles. This figure demonstrate that ruptures have clear tendency to be initiated in areas of small Dc values. This can be confirmed by histogram in Fig.6b, which compare probability distribution of Dc values on the fault (blue), with the distribution of Dc values at rupture initiation points (orange). Around 70% of ruptures are initiated at small $Dc < 0.2Dc\_max$.

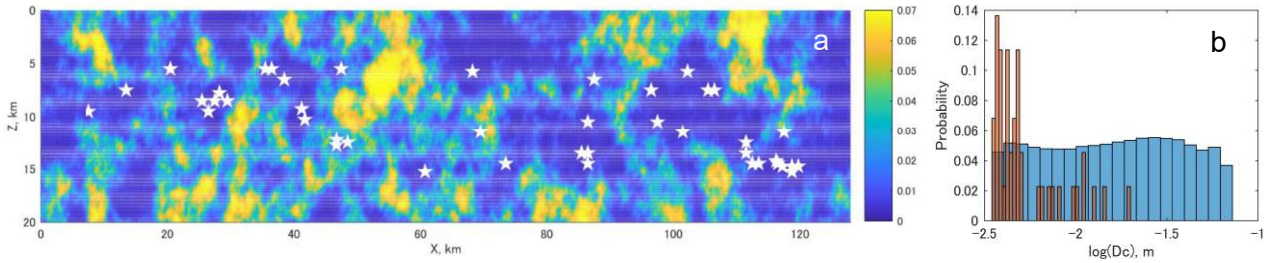

Fig. 6 – Left: *Dc* distribution and rupture initiation points (stars). Right: histograms of *Dc* values (blue) and *Dc*'s at rupture initiation points (orange). Most of ruptures are initiated in small *Dc* areas

5. Analysis of the poorly observed rupture parameters

5.1 Stress drop

In [1] we succeed to tune *S* vs *Mo* scaling by tuning of stress drop. Fig.7 shows average stress drop Δσ values vs *Mo* for the screened rupture models above. Estimated average is 3.2 MPa. This value is almost the same as Δσ = 3.1 MPa estimated in [5], and Δσ = 3.0 MPa assumed by the Recipe in Japan. Scattering of Δσ values is large and in average, Δσ doesn't change with increasing of magnitude through the 1st to 2nd stage transition, although a little tendency to decrease exists. For ruptures in the 1st stage with $Mw < 6.5$ average Δσ = 3.5 MPa, while for ruptures in 2nd stage with $Mw > 6.5$ Δσ=2.3 MPa. This difference agrees with results [25, 26] that surface ruptures may have smaller Δσ values than buried ruptures.

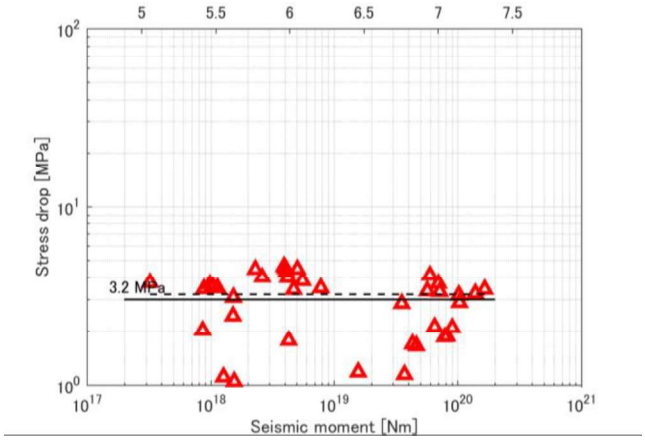

Fig. 7 – Scaling of the average stress drop in rupture area. Lines are the average Δσ (dashed) and Δσ value assumed in Recipe (solid)

5.2 Slip rate function

Strong ground motion predictions using kinematic models for the scenario earthquakes require SRF settings. SRF can be estimated from the multi-time window seismic source inversion results, numerical dynamic simulations or theory. Due to limited resolution, estimated from source inversions SRF have lack of high frequency content. Numerical SRFs estimated from validated dynamic models like in this study, are more reliable. In a previous numerical simulation studies, e.g. [27, 28], numerical SRFs were approximated by an analytical function. In this paragraph we analyze numerical SRFs approximated by the Regularized Yoffe function (RYF [3, 11]).

At first step we calculate average SRFs inside each 1x1km subfault. Background subfaults having maximum *PSR* < 3% of maximum *PSR* of the whole rupture were excluded from analysis. Then, each numerical SRF were approximated by RYF, see example in Fig.8a. RYF is described by two time parameters: half-width of smoothing window *Ts* and rise time *Tr*. Peak delay time of RYFs in Fig.8a can be

approximated as 1.3*Ts* [11]. Examples of distributions of *Ts* and *Tr* are shown in Fig.8b and c. In most subfaults SRF has Kostrov shape: typical high-speed rise in a less than 1 sec interval, and then gradual decrease in a few seconds, sometimes with a little flattening before final drop to almost zero amplitude. However, in some subfaults (e.g. see right side of the rupture initiation point) SRF has smooth ramp function shape with large *Ts* and *Tr* values. This kind of SRFs is observed frequently at the near surface subfaults too. Below we will analyze these features in relation with distributions of other dynamic parameters.

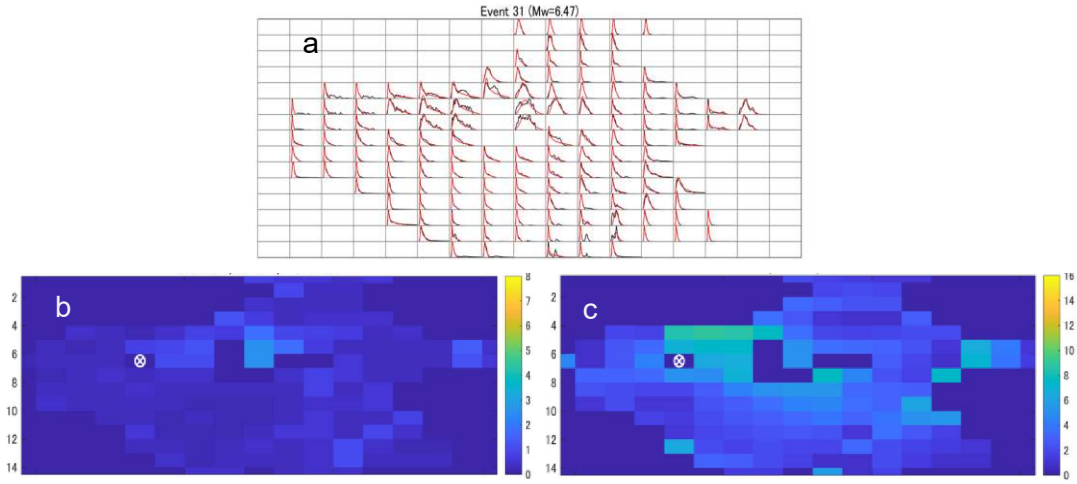

Fig. 8 – Example of SRF analysis. (a) average simulated SRF for the 1km meshes (black) and the fitting of the regularized Yoffe function (RYF, red). (b) distribution of the peak delay time Ts of RYF's. (c) distribution of the rise time Tr of RYF's

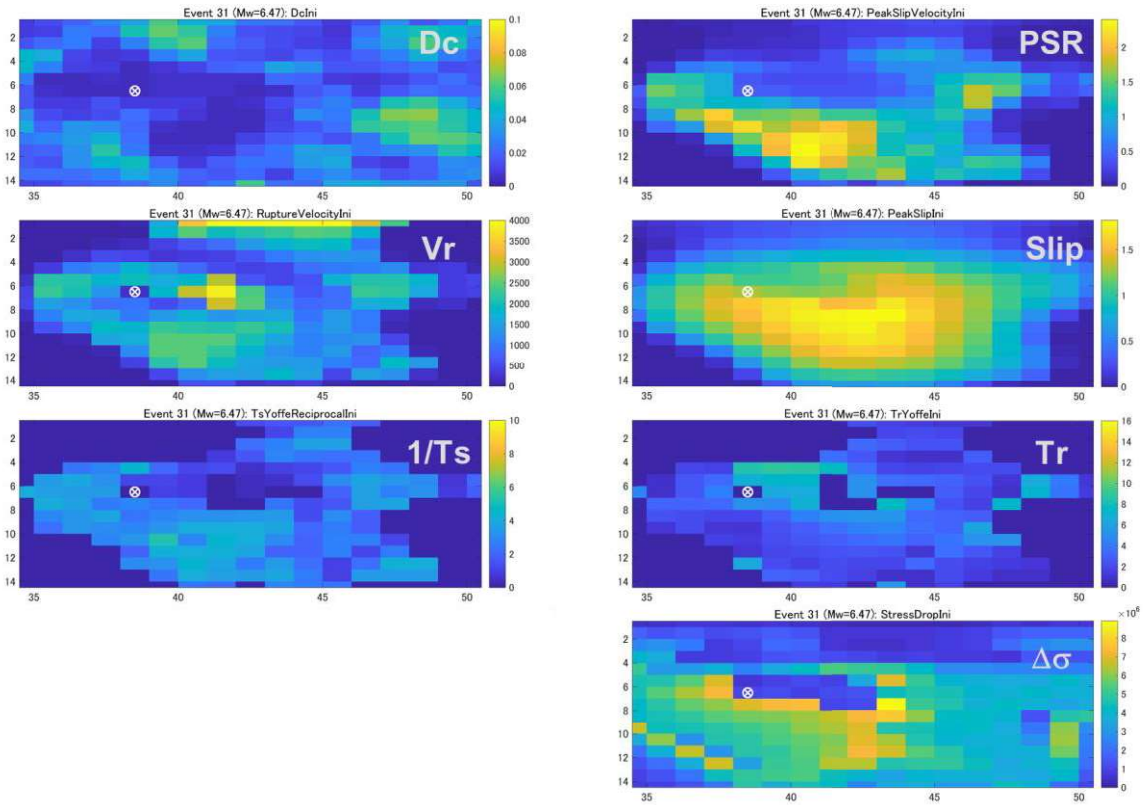

Fig. 9 – Example of comparison of distributions of key rupture parameters that suppose existence of cross-correlation between them. White circle – rupture initiation point

5.3 Cross correlations between parameters

Fig.9 shows distribution examples of some key parameters: *Dc*, *PSR*, peak slip, *Vr*, *Ts*, *Tr* and Δσ, for *Mw*6.47 event. *Dc* is the only heterogeneous friction parameter in this study, other parameters are rupture parameters important for kinematic source modelling for strong motion prediction. It seems that there are spatial correlations between parameters: high *PSR* areas correlate with areas of small *Dc*, large rupture velocity and small *Ts*-time, area of large *Tr* correlate with small *PSR* and small Δσ. Although there can be a spatial offset in some cases. In this paragraph we explore these spatial correlations by the spatial coherence method with non-zero offset proposed in [9, 10]. In contrast to [9], *PSR* but not peak slip, is selected as a primary parameter and spatial correlations of *PSR* with other parameters (*Vr*, *Dc*, peak slip and *Ts*) are explored.

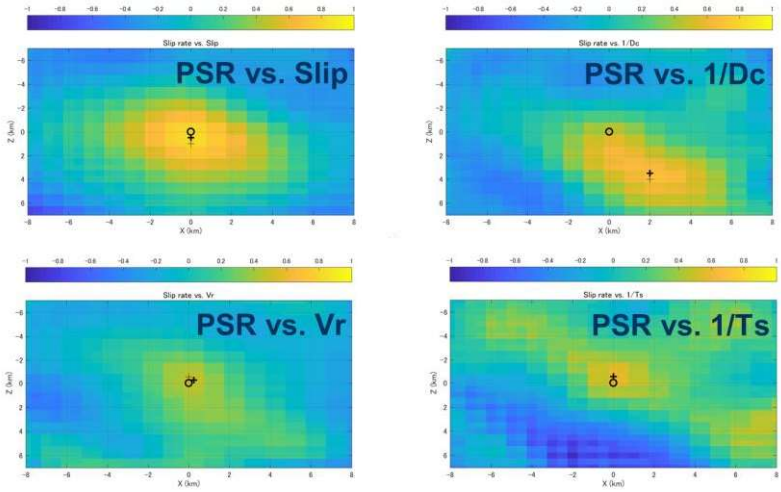

Fig. 10 – Example of cross-correlation analysis for the rupture in Fig.9. *PSR* is selected as a primary parameter. Circle marks point of zero shift between parameters, plus mark indicates shift with maximum cross-correlation. X and Y axes are shift in km, in strike and dip directions respectively, between the target parameter distributions shown in title

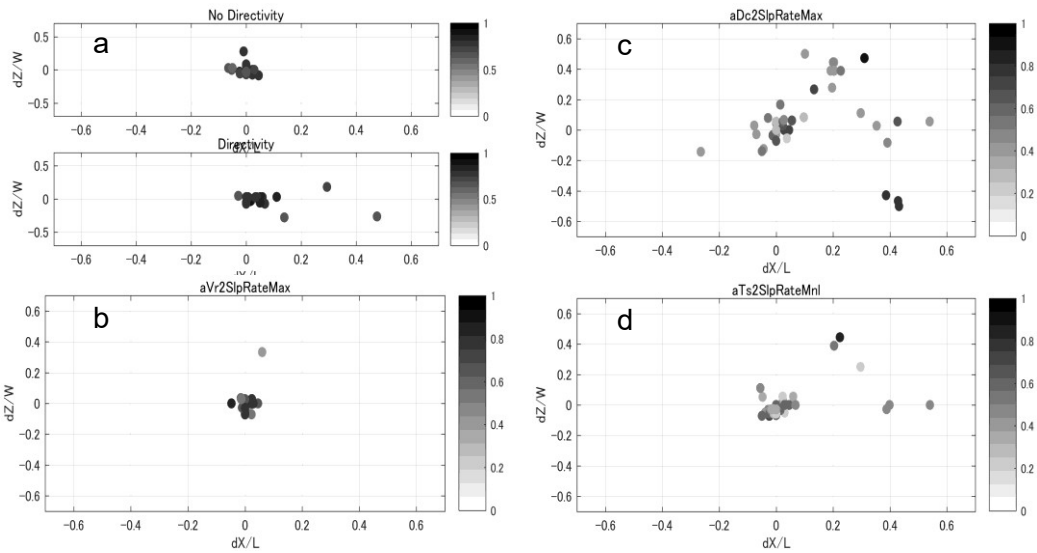

Fig. 11 – Spatial shift and correlation value at the peaks of cross-correlation for all rupture models, for parameter pairs in Fig.10. Dots indicate spatial shift between parameters. The color of dots indicates maximum correlation coefficient values. X and Y axes are normalized shift in strike and dip directions respectively, between the target parameter distributions

Fig.10 shows examples of the spatial correlation structure for event in Fig.9. X and Y axes are the spatial shift between spatial distributions of parameters, color indicate correlation strength. The spatial correlation analysis shows that there are strong correlation peaks between peak slip rate and other parameters. Null offset exists for correlations with slip and *Vr*, non-zero offset for correlation with *Dc*. Spatial correlation with 1/*Ts* shows pattern with several peaks. Existence of several peaks was observed in other rupture models too. Central peak is not necessary the largest peak. We made visual inspection of all correlation patterns. In case if largest peak is far from center, but another strong peak exists closer to center, we prefer this second peak as the measure of spatial correlation. In order to avoid this kind of manual selection, a weighted procedure with weight proportional to *PSR* value, is necessary for future work.

Fig.11 compiles amplitude and offset values of the cross-correlation peaks for all rupture models. Rupture propagation direction affects the horizontal shift of the location of the correlation peak. Specifically, if the hypocenter is located on the right side of rupture area, the maximum correlation is located on the left side, and vice versa. In order to account for this directivity effect, we changed propagation direction of ruptures so that all directivity would be aligned from left to right. Additionally, we assigned "no directivity" to ruptures that have hypocenter inside the large slip area.

Analysis of spatial correlation between *PSR* and peak slip in Fig.11a demonstrates that areas of large *PSR* and peak slip are coinciding in "no directivity" cases. Ruptures with "directivity" have small (less than 10% of rupture length) but systematic offset in directivity direction: high rate area is shifted to the outer edge of large slip area. Only in 4 cases this shift larger than 10%. Relatively small offset may be related to small magnitudes of studied ruptures and exclusion of the edge arrested ruptures during the screening.

In contrast to results in [9] for example, spatial correlation between *PSR* and *Vr* in Fig.11b has no shift of correlation for all studied ruptures. This is theoretically expected result, see [29]. Disagreement with *Vr* estimated by source inversion probably reflect the fact that spatial distribution of *Vr* is poorly resolved by the multi-time-window inversion having just a few windows.

Spatial correlations between *PSR* and 1/*Dc* in Fig.11c has two large groups. More than half of ruptures (around 59%) have near zero offset. This important result indicates that SMGA, which is associated with high-rate area, may keep location in earthquake cycles on the same geological fault. The rest of ruptures (41%) may have offset of high-rate area in the directivity direction.

Similar to correlation with 1/*Dc*, peaks of spatial correlation between *PSR* and 1/*Ts* in Fig.11d also have two groups. Around 86% of ruptures have near zero offset, and only 14% of ruptures have offset of high-rate area in the directivity direction. This is expected result also: under smooth slip condition, short *Ts* values (large 1/*Ts*) result in large *PSR* values.

This analysis provides evidence that offset of maximum correlations between earthquake source parameters is smaller than could be expected from analysis of source inversion models in [9, 10]. Although a larger non-zero response distance of temporal rupture parameters with respect to *PSR* may exist for large characteristic strike-slip events with $Mw > 7.5$.

6. Discussion

Simulated events are a valuable data set for the study of detailed features of rupture models. Here we confirmed that there may be significant correlations between slip rate, rise time, rupture velocity and *Dc* distribution. There are also indications that the other parameters in Fig.9, *Tr* and $\Delta\sigma$ as well as other parameters not mentioned here, also have correlations with *PSR* and *Dc*. These will be analyzed in future work.

In our simulations, *Dc* is the only heterogeneous model parameter. Heterogeneity of stress drop and strength excess is the spontaneous result of earthquake cycles. For this reason, correlations with *Dc*, the only parameter that remains unchanged throughout multiple cycles, are most important. They may allow us to

extrapolate features observed in past earthquakes into future earthquakes on the same geological fault and reduce uncertainty of strong motion predictions.

7. Conclusions

Large number of physics-based rupture models, both for small and large events with *Mw*5.5~7.5, simulated self-consistently in earthquake cycles, were successfully validated by comparison with observed source scaling relationships, permanent surface offset and ground motion's *PGV* (through GMPE). Scaling relations of simulated ruptures for rupture area *S* and average slip *Dave* vs. *Mo* clearly confirms transition between 1st and 2nd stages, which correspond to the self-similar and width-saturated models respectively. Average $\Delta\sigma$ agrees with the value proposed in Recipe: $\Delta\sigma$ = 3.0MPa. By analysis of rupture parameters we confirm or re-evaluate that: (1) ruptures have strong tendency to be initiated in areas of small *Dc*, (2) for ruptures in the 1st and 2nd stages, peak slip rate distributions correlate with peak slip distributions, possibly with a minor spatial offset, (3) peak slip rate correlates well without any offset with rupture velocity, (4) in most of cases, large peak slip rate areas correlate with small *Dc* areas, (5) distribution of peak delay time of the slip rate functions also correlates well with the peak slip rate without spatial offset.

8. Acknowledgements

This study is based on the 2018 research project 'Examination for uncertainty of strong ground motion prediction for inland crustal earthquakes' by the Secretariat of Nuclear Regulation Authority (NRA), Japan. Many thanks to Toshimitsu Nishimura for providing us set of subroutines for GMPE calculation.

9. References

[1] Galvez P, Petukhin A, Somerville P, Miyakoshi K, Irikura K (2020): Heterogeneous Multicycle Dynamic Rupture Modeling for a Vertical Strike-Slip Fault. *17th World Conference on Earthquake Engineering, September 13-18, Sendai, Japan*, Submitted.

[2] Irikura K, Miyake H (2011): Recipe for predicting strong ground motion from crustal earthquake scenarios. *Pure Appl. Geophys.*, **168**, 85, doi:10.1007/s00024-010-0150-9.

[3] Schmedes J, Archuleta RJ, Lavallee D (2010): Correlation of earthquake source parameters inferred from dynamic rupture simulations. *J.Geophys.Res.*, **115**, B03304, doi:10.1029/2009JB006689.

[4] Field EH (2019): How physics-based earthquake simulators might help improve earthquake forecasts. *Seismol. Res. Lett.*, doi.org/10.1785/0220180299.

[5] Fujii Y, Matsu'ura M (2000): Regional Difference in Scaling Laws for Large Earthquakes and its Tectonic Implication. *Pure Appl. Geophys.*, **157**, 2283–2302.

[6] Matsu'ura M, Sato T, (1997): Loading Mechanism and Scaling Relations of Large Interplate Earthquakes. *Tectonophysics*, **227**, 189–198.

[7] Luo Y, Ampuero JP, Miyakoshi K, Irikura K (2017): Source rupture effects on earthquake moment-area scaling relations. *Pure Appl. Geophys.*, **174**, 3331, doi: 10.1007/s00024-017-1467-4.

[8] Mai PM, Beroza GC (2002): A spatial random field model to characterize complexity in earthquake slip. *J. Geophys. Res.*, **107**, doi:10.1029/2001JB000588.

[9] Song SG, Pitarka A, Somerville P (2009): Exploring Spatial Coherence between Earthquake Source Parameters. *Bull. Seismol. Soc. Am.*, **99** (4), 2564–2571.

[10] Song SG, Somerville P (2010): Physics-Based Earthquake Source Characterization and Modeling with Geostatistics. *Bull. Seismol. Soc. Am.*, **100** (2), 482–496.

[11] Tinti E, Fukuyama E, Piatanesi A, Cocco M (2005): A Kinematic Source-Time Function Compatible with Earthquake Dynamics. *Bull. Seismol. Soc. Am.*, **95**, 1211–1223, doi: 10.1785/0120040177.

[12] Somerville P, Irikura K, Graves R, Sawada S, Wald D, Abrahamson N, et al. (1999): Characterizing crustal earthquake slip models for the prediction of strong ground motion. *Seism. Res. Lett.*, **70**, 59-80.

[13] Irikura K, Miyake H (2001): Prediction of strong ground motions for scenario earthquakes. *Journal of Geography (Chigaku Zasshi)*, 110(6), 849–875.

[14] Dreger DS, Beroza GC, Day SM, Goulet CA, Jordan TH, Spudich PA, Stewart JP (2015): Validation of the SCEC Broadband Platform V14.3 Simulation Methods Using Pseudospectral Acceleration Data, *Seism. Res. Lett.*, **86**, 39.

[15] Graves RW, (1996): Simulating seismic wave propagation in 3D elastic media using staggered-grid finite differences. *Bull. Seismol. Soc. Am.*, **86**, 1091.

[16] Pitarka A, (1999): 3D elastic finite-difference modeling of seismic motion using staggered grids with nonuniform spacing. *Bull. Seismol. Soc. Am.*, **89**, 54.

[17] Bouchon M (1981): A Simple Method to Calculate Green's Function for Elastic Layered Media. *Bull. Seismol. Soc. Am.*, **71**, 959.

[18] Boore DM, Stewart JP, Seyhan E, and Atkinson GA (2014): NGA-West2 equations for predicting PGA, PGV, and 5% damped PSA for shallow crustal earthquakes. *Earthquake Spectra*, **30,** 1057.

[19] Koketsu K, Miyake H, Suzuki H (2012): Japan Integrated Velocity Structure Model Version 1. *15th World Conference on Earthquake Engineering, Lisbon, Portugal, 24-28 September*, Paper 1773.

[20] Petukhin A, Kagawa T, Koketsu K, Miyake H, Masuda T, Miyakoshi K (2012): Construction and waveform testing of the large scale crustal structure model for Southwest Japan. *15th World Conference on Earthquake Engineering, September 24-28, Lisbon, Portugal*, paper 2789.

[21] Si H, Midorikawa S (1999): Attenuation Relations for Peak Ground Acceleration and Velocity Considering Effects of Fault Type and Site Condition. *Journal of Struct. Construct. Eng. (Transactions of AIJ)*, **523**, 63 (in Japanese).

[22] Petersen MD, Dawson TE, Rui Chen, Tianqing Cao, Wills CJ, Schwartz DP, Frankel AD, (2011): Fault Displacement Hazard for Strike-Slip Faults. *Bull. Seismol. Soc. Am.*, **101**, 805–825, doi: 10.1785/0120100035.

[23] Stirling M, Rhoades D, Berryman K (2002): Comparison of earthquake scaling relations derived from data of the instrumental and pre-instrumental era. *Bull. Seismol. Soc. Am.*, **92**, 812–830.

[24] Murotani S, Matsushima S, Azuma T, Irikura K, Kitagawa S (2015): Scaling Relations of Source Parameters of Earthquakes Occurring on Inland Crustal Mega-Fault Systems. *Pure Appl. Geophys.*, **172**, 1371–1381.

[25] Somerville PG (2003): Magnitude scaling of the near fault rupture directivity pulse, *Phys. Earth Planet. Int.*, **137**, 201–212.

[26] Kagawa T, Irikura K, Somerville PG (2004): Differences in ground motion and fault rupture process between the surface and buried rupture earthquakes. *Earth Planets Space*, **56**, 3–14.

[27] Nakamura H, Miyatake T (2000): An approximate expression of slip velocity time functions for simulation of near-field strong ground motion. *Zisin (J. Seismol. Soc. Jpn.)* **53**, 1–9 (in Japanese with English abstract).

[28] Bizzarri A, (2012): Analytical representation of the fault slip velocity from spontaneous dynamic earthquake models. *J. Geophys. Res.*, **117**, B06309.

[29] Gabriel AA, Ampuero JP, Dalguer LA, Mai PM, (2012): The transition of dynamic rupture modes in elastic media. *J. Geophys. Res.*, **117**, 0148-0227, doi: 10.1029/2012JB009468.

